







An Output-sensitive Algorithm for Generating Island Scanning Paths with Applications in SLM Additive Manufacturing

Ruiliang Feng¹ , Lin Zhu² , Peng Li³ , and Xiangzhi Wei⁴ 

¹Shanghai Jiao Tong University, fengruiliang@sjtu.edu.cn

²Shanghai Jiao Tong University, zhulin0728@sjtu.edu.cn

³Shanghai Aerospace Equipments Manufacturer Co., Ltd, lipeng314159@126.com

⁴Shanghai Jiao Tong University, antonwei@sjtu.edu.cn

Corresponding author: Xiangzhi Wei, antonwei@sjtu.edu.cn

Abstract. Selected Laser Melting (SLM) is a major type of technique of Additive Manufacturing for fabricating complicated 3D metal models that are used in aeronautic, medical and automotive industries. Island scanning strategy has been shown to be an effective means for melting the metal powders into solids with less distortion and cracking. However, existing literature and the handouts of the commercial software have not shown how to compute the island scanning strategy effectively for a large number of layers of a 3D printed model. In this paper, we propose an output-sensitive algorithm for generating the island scanning paths for one layer, with taking $O(K + M)$ times, where K is the number of laser paths in the interior the layer and M is the total number of contour edges of slice. The algorithm has been integrated into our self-developed software “Meshprint”. Three examples were simulated in “Meshprint” and were 3D printed using an SLM machine, the results validated our proposed algorithm.

Keywords: Additive Manufacturing, path planning, island scanning strategy.

DOI: <https://doi.org/10.14733/cadaps.2020.752-762>

1 INTRODUCTION

Selective Laser Melting (SLM) [11], a type of technology of Additive Manufacturing, fabricates metal part by progressively adding thin layers of materials. For each layer, the laser melt and solidify a selective region of metallic powder by moving along infill paths that has been compute from a CAD model [3]. Due to this feature, SLM can directly product complex or customized 3-dimensional parts that cannot be obtained using conventional process, and is mainly used in manufacturing mechanical products with applications in the aeronautic [16], medical [5] and automotive industry [4].

However, different from other Additive Manufacturing techniques such as Fused Deposition Modeling (FDM) and Stereolithography Apparatus (SLA), the SLM method generates larger spatial

temperature gradients around the melting region. Due to the moving velocity of the laser is 10-1000 mm/s, the temperature of the melting region that hit by the intense laser rises rapidly, and is significantly higher than its adjacent region. The melting region is in a thermal expansion state while its adjacent regions are under thermal contraction. They restrict each other during the whole laser-scanning process. This phenomenon is the major cause of residual stress [19-20] in the final SLM components [17].

The introduced residual stresses can cause the part failure due to part distortion [8], cracking [7] (see Figure 1) during depositing, and there will be emerging delamination defect [15] (i.e., separation of two consecutive layers) once the induced residual stress exceeds the yield strength of the alloy. Other effect of residual stresses is that the fatigue and fracture resistance of the parts are decreased [9],[12].

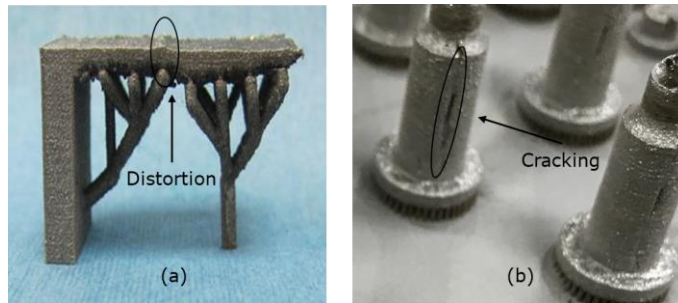


Figure 1: The defects in a SLM part: (a) Distortion, and (b) Cracking.

To reduce the residual stress, a lot of methods have been explored, these include but are not limited to preheating substrate [1], adding support structure for overhang [6],[14],[22], heat treatment [12], and adjusting scanning parameters. The scanning parameters include scanning velocity, spot size and scanning power and the scanning strategy. Refer to Figure 2, there are three commonly used scanning patterns: unidirectional scanning strategy, bi-directional scanning strategy and island scanning strategy (or sectoral scanning strategy).

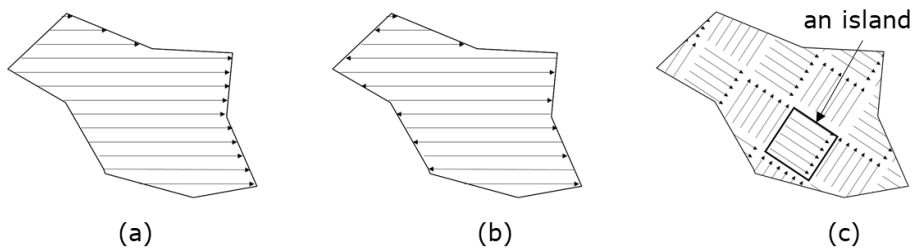


Figure 2: Scanning strategies: (a) Unidirectional scanning pattern, (b) Bi-directional scanning pattern, (c) Island scanning pattern.

The investigations of [12] and [8] found that when using unidirectional scanning strategy, deformations along scanning direction is less than those perpendicular to the scanning direction, and that when using island scanning pattern deformations along each of these directions is fairly small. They also showed that when fabricating a cuboid with unidirectional scanning strategy, scan parallel the long side of the cuboid introduces larger stress than parallel the short side, while the island scanning strategy yielded an intermediate stress level; in addition, scanning a region for a second time using 50% of the laser power can reduce the tensile stress of the part. Particularly,

Yasa et al. [21] found that island scanning pattern reduced the residual stress significantly for bridge-like parts; Lu et al. [10] investigated the influence of the size of island on the density, hardness, mechanical property and residual stress in Inconel-718 alloy parts. However, island scanning strategy introduced more paths than the existing path strategies. This means that laser take more time in turning amongst path segments. therefore, compared with other scanning strategies (e.g., Unidirectional scanning pattern and Bi-directional scanning patter), the island scanning strategy takes more printing time.

In terms of microstructures, Thijs et al. [18] studied the microstructure and controllable texture of SLM AlSi10Mg parts fabricated with the island scanning strategies; Carter et al. [2] found cracks appeared in the repeating fine-grained regions in grain orientations that was caused by shifting the island scanning pattern, and they suggested to determine the scanning strategy in layer-by-layer manner according to the geometric features of part.

In term of generating island scanning paths, in 2009, Zhang et al proposed an algorithm for computing the island scanning paths [23], which calculated the intersections of parallel lines with the contour edges of each slice, and paired these intersection points into lines, and finally broke up those lines into island paths at island boundaries.

In this paper, we further improve Zhang's algorithm by reducing the amount of calculations for the intersections of parallel lines with contours. We also propose a strategy of generating a rotated island scanning strategy for a sequence of slices, which is used in most practical fabrication processes of SLM.

The rest of the paper is organized as follows: Section 2 presents our algorithm; Section 3 presents our self-developed "Meshprint" and simulates three models; finally, section 4 presents the conclusion and limitation of this algorithm.

2 ALGORITHM AND COMPLEXITY

To begin with, some terminologies are introduced for the brevity of illustration. As shown in Figure 3, a square filled with a series of parallel paths is called *island*. The length of island along U is W , and the length of island along V is H . There are two kinds of islands: one is filled with a set of parallel paths directed along U , for brevity we call it *Type I island*; the other is filled with a set of paths directed along V , we call it *Type II island*. The variable Δ is used to present the gap between two neighboring paths in an island.

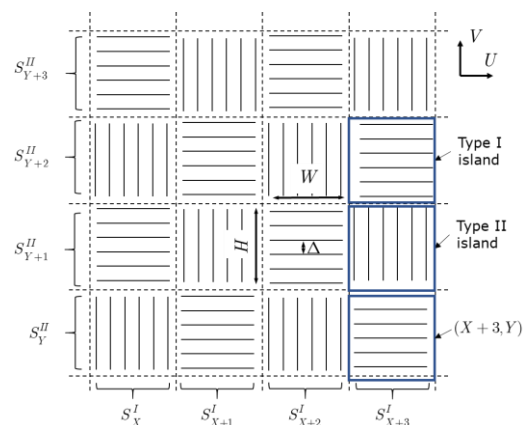


Figure 3: Illustration of the islands: each island is denoted by (X, Y) , which is a region of the intersection of S_X^I with S_Y^{II} ; S_X^I is X^{th} strip directed along U and S_Y^{II} is Y^{th} strip directed along V ;

type I island contains parallel paths directed along U , type II island contains parallel paths directed along V .

As illustration in Figure 3, in this paper, an island is denoted by (X,Y) , where X is the index of type I strip directed along U , and Y is the index of type II strip directed along V . If $(X+Y)$ is an odd number, then it is a Type I island, otherwise is a Type II island. For example, the lower right corner island in Figure 3 is presented as $(X+3,Y)$ and it is a type I island. Notice that the difference between the value of $(X+Y)$ of two adjacent islands is 1, which ensures that the infill patterns in these two neighboring islands are perpendicular.

Before presenting the island generation algorithm, some critical definitions are given as below: The input data is a slice of model which is presented by a set of connected components $C := \{C_1, C_2, \dots, C_i, \dots, C_m\}$. As shown in Figure 4, the slice has three connected components. A connected component C_i , is a simply polygon which is represented by a sequence of directed edges $\partial C_i := (e_1, e_2, \dots, e_i, \dots, e_n)$, where the outer contour is represented in counter-clockwise order and the inner contour is represented in clockwise order; in this manner the interior of connected component C_i is on the left of each edges.

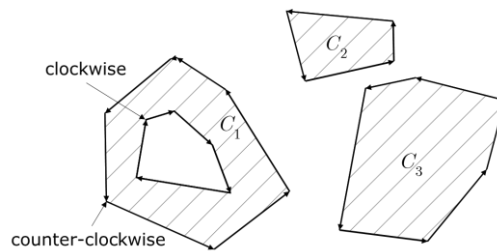


Figure 4: A slice which has three connected components.

The main idea of generating island paths for any slice is as follows: For each connected component in the slice, determine the islands that are penetrated by the boundary edges of the slice, and then start from founded islands, determine the pattern (horizontal or vertical) of all islands that are interior to this connected component. The details of this algorithm are given as follows:

Algorithm Generate_Island_Paths (C)

Input: A slice represented by a set of connected components, $C := \{C_1, C_2, \dots, C_i, \dots, C_m\}$.

Output: Island scanning paths for all islands that are interior to slice C .

1. **for** each $i := 1$ to n **do**
 2. **for** each edge $e \in \partial C_i$ **do**
 3. determine islands that are penetrated by e and mark them as boundary islands;
 4. start from marked island, infill the islands with vertical or horizontal paths that are interior to C_i in a Breadth First Search (BFS) manner;
 5. **return** island scanning paths for all islands that are interior to slice C ;
-

The details of this algorithm is presented as the following organization : section 2.1 presents how to determine a sequence of islands that are penetrated by an edge; section 2.2 presents how to infill island in a Breadth-First-Search manner; section 2.3 will analysis the time complexity of this algorithm.

2.1 Determine Islands crossed by a Contour Edge

Given a contour edge e , if the absolute value of the slope of e is not larger than H/W , starting from the origin of e , generate points on e by an interval of W along U ; otherwise, generate the points at an interval of H along V . For each point generated and each endpoint of s , we use Eq. (2.1) and Eq. (2.2) to determine which island it belongs to.

$$X = \lfloor x/W \rfloor \quad (2.1)$$

$$Y = \lfloor y/H \rfloor \quad (2.2)$$

where x and y are the coordinates of a point.

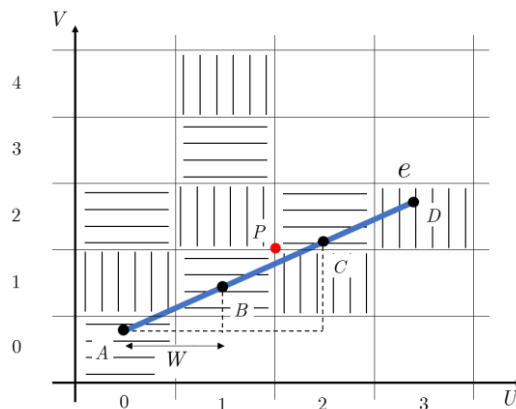


Figure 5: Illustration of the islands crossed by edge whose absolute value of the slope is not larger than H/W .

For the case that two consecutive points on e locate in (X,Y) and $(X+1,Y+1)$, it is necessary to check whether $(X+1,Y)$ or $(X,Y+1)$ is crossed by e . If the lower-left corner of $(X+1,Y+1)$ is higher than e , then $(X+1,Y)$ is crossed; otherwise, $(X,Y+1)$ is crossed. For example, B and C (as shown in Figure 5) are located in island $(1,1)$ and $(2,2)$ respectively, point P is higher than e , then the lower island $(2,1)$ is crossed. For ease of description, during the process of determining islands for contour edges, for each island (X,Y) , we use $L(X,Y)$ to store the contour edges that cross through island (X,Y) .

2.2 Generate Island Patterns for a Connected Component by BFS

Line 3 in **Algorithm Generate_Island_Paths (C)** has marked all the boundary islands for C_i . Starting from those islands, BFS is called to mark their neighboring islands that are interior to C_i .

During the searching process, every new marked island is infilled with horizontal or vertical paths. Figure 6 shows the searching process for a connected component.

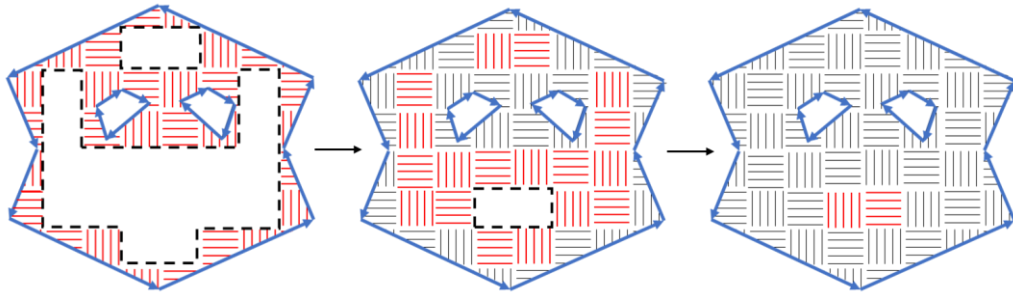


Figure 6: Illustration of the searching process for a connected component: The left figure shows all the islands (in red) that cross the boundaries of C_i , where the boundaries (dashed line) of the unmarked regions are dashed; The middle figure shows the newly marked islands (in red) by BFS starting from the dashed boundaries in the left figure; the right figure shows the newly marked islands by BFS starting from the dashed boundaries in the middle figure.

In particular, to determine paths (the red line segments in island of Figure 7) for an island crossed by a number of contour edges, we split paths in this island into segments and only keep those are on the left of each edges.

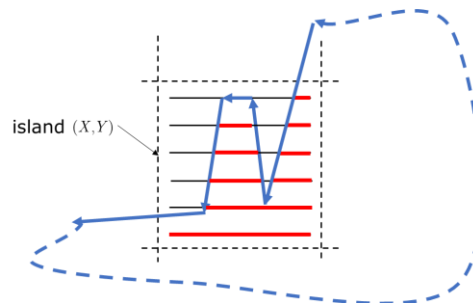


Figure 7: Illustration of generating paths: Red segments are the infilled paths. For island (X,Y) that is crossed by a set of edges, paths are split and only those on the left of $L(X,Y)$ are kept.

2.3 Complexity Analysis and The Improvement of This Algorithm

This algorithm has a total time complexity of $O(K + M)$, where K is the number of paths in the interior of the slice, and M is the number of edges on the boundary of the slice. The details of analysis are given below.

The step of determining islands for the contour of a connected component takes $O(m + n)$, where m is the number of contour edges, and n is the number of islands that are crossed by the contour. Searching islands for the interior of this connected component takes $O(n')$, where n' is the number of islands that are interior to the connected component. The step of generating paths for an island takes $O(k)$ time, where k is the number of output paths in this island.

In conclusion, for a slice with a set of connected components, the algorithm takes $O(K + M)$ time, where K is the total number of paths in slice and M is the total number of contour edges of slice. The running time is proportional to the number of the output segments, which means that the algorithm is output-sensitive.

The improvement of this algorithm comparing with existing algorithm such as Zhang's [23] is that it reduces the time of computing the intersection of parallel lines with the boundary edges. In Zhang's algorithm, the intersection with horizontal and vertical lines are both been computed for every contour edge; As a contrast, in our algorithm, by judging what kind of island is crossed by edge, only the intersection of it with horizontal or vertical line in island are computed.

3 THE SELF-DEVELOPED "MESHPRINT" SOFTWARE AND EXAMPLES

This algorithm has been integrated into our self-developed SLM software, "Meshprint", which is developed in C++ language with Qt library and OpenGL API. Figure 8 shows the main interface where the left column is the window for the geometric parameter setting of the support structures, island scanning parameter settings and the laser parameter settings. The right column of this interface is used to render models and inspect the scanning paths. The window of island parameter settings offers users to tune not only the width and length of islands, but also the overlap distance between two neighboring islands and the interval between adjacent path segments. Note: A demonstration video of the software is available in the link [13].

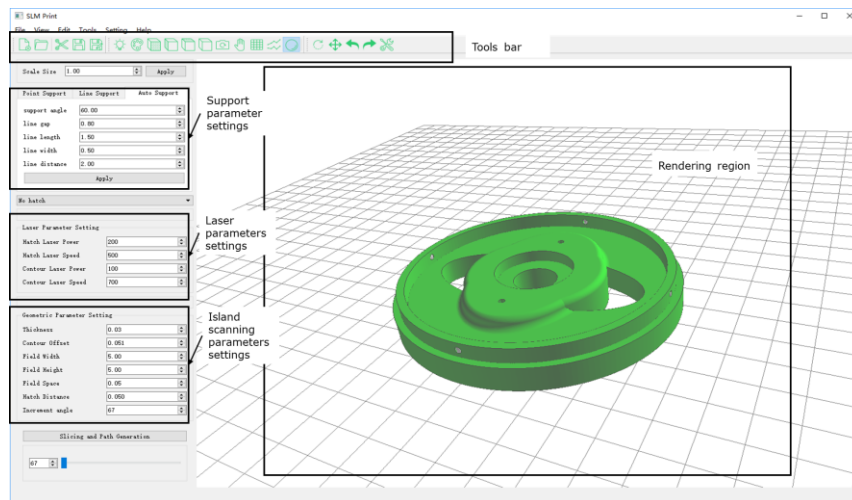


Figure 8 : The main interface of "Meshprint" with the windows for the settings of laser and island scanning parameters.

3.1 Spinning up the Island Scanning Pattern

"Meshprint" allows to rotate the island scanning paths in a layer-by-layer manner, where the incremental rotation angle is α . The pattern of upper layer is obtained by rotating the pattern of the lower layer by an angle of α in the counterclockwise direction.

Note that **Algorithm Generate_Island_Paths** (C) only works for regular background patterns with vertical and horizontal lines, in order to compute the paths of contour C with a rotated island pattern (Figure 9(a)) we need to adapt it as follows: first of all, we rotate the background pattern by an angle of α in clockwise order (Figure 9 (b)); and then we rotate the contour C by an angle

of α in the clockwise direction (Figure 9 (c)), and then we use **Algorithm Generate_Island_Paths** (C) to generate islands enclosed in the inter of C ; finally, we rotate C and the background pattern together by an angle of α in the counterclockwise direction.

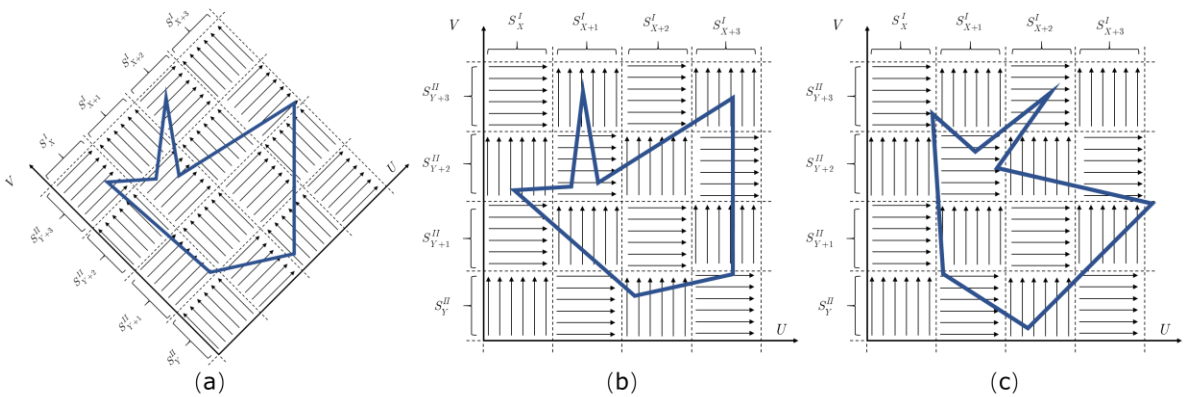


Figure 9 : Illustration of rotating island scanning paths by an angle of α : (a) The target state, (b) The background pattern is rotated by an angle of α in the clockwise direction, (c) The contour C is rotated by an angle of α in the clockwise direction. The positions of the islands enclosed in C in Figure 9(c) are different from those enclosed in C in Figure 9(a) by an angle of α .

3.2 Examples

In this subsection, refer to Figure 10-12, three models are simulated in “Meshprint”, the images in each figure contains the effects of loading models, generating support structures, and island scanning path planning. “Meshprint” provides “point support” as the support structure and the paths in the interior of support structure are rendered in red, and the paths in the interior of model are rendered in black.

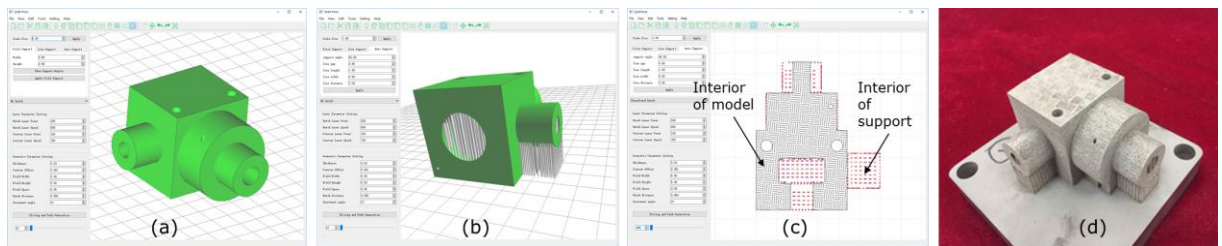


Figure 10: The simulation of Model I using our self-developed “Meshprint” software: (a) The input model, (b) The supported model, (c) The inspection of paths of 395th layer, (d) The SLM 3D printed part.

3.3 Comparing with Existing Algorithm

On a computer with Intel® Core™ i7-4770K @ 3.50GHZ and 8GB RAM, we compared the running time of “Meshprint” with the island scanning function of the path planning module of Materialise. Materialise is a company that specializes in developing software for Additive Manufacturing. It can be seen from Table 1 that “Meshprint” consumes less time, saving about 70%-80%. However, Magics also has own advantages since it is compatible with various scanning strategies. In addition,

we compared the running time of “Meshprint” with the Zhang’s algorithm and “Meshprint” saving about 20%-30% time.

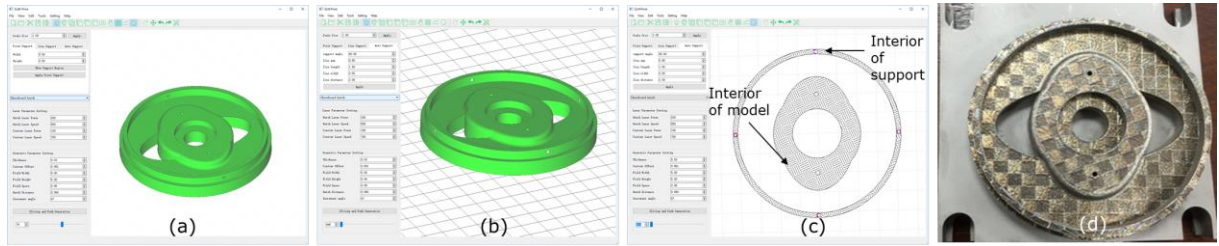


Figure 11: The simulation of Model II using our self-developed “Meshprint” software: (a) The input model, (b) The supported model, (c) The inspection of paths of 280th layer, (d) The SLM 3D printed part.

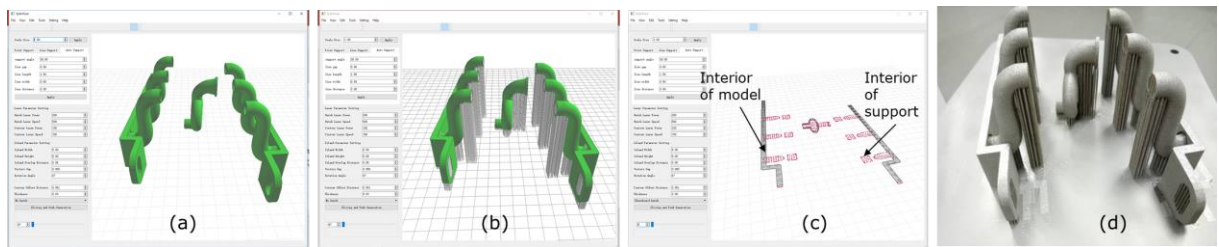


Figure 12: The simulation of Model III using our self-developed “Meshprint” software: (a) The input models, (b) The supported model, (c) The inspection of paths of 202th layer, (d) The SLM 3D printed part.

Test model	Dimension (mm×mm×mm)	Number of triangles	Number of layers	Consuming time of Magics	Consuming time of Zhang’s (s)	Consuming time of Meshprint (s)	Save time (VS Magics)	Save time (VS Zhang’s)
Model I	60×71.5×44	32444	1467	24.00	7	5.2	72%	25%
Model II	93×89×13	22384	400	9.0	1.5	1.2	85%	20%
Model III	135×192.7×71.5	45176	2383	28.0	7.5	5.3	73%	29%

Table 1: The comparison between our self-developed “Meshprint” software with Zhang’s algorithm and the island path canning modules of Materialise.

4 CONCLUSION

Island scanning strategy is an effective means in reducing the residual stress to produce SLM parts with less warpage and cracking. However, the literature and handouts of the commercial software for efficiently computing the island scanning path is rare. In this paper, we propose an output-sensitive algorithm for generating the island scanning paths, which has been successfully integrated into our self-developed software “Meshprint”. This algorithm outperforms the Zhang’s algorithm.

However, our work also suffers from some limitations, and the following are some potential directions for future research:

1. The proposed algorithm only works on models without any non-manifold errors such as facet intersections, normal inverse.
2. The current work only considers the geometric computation; a comprehensive understanding of the interaction of the geometric patterns and laser parameters can help reduce the influence of the residual stress.
3. An improvement may be achieved by learning the scanning strategies from exiting layers to help determine the subsequent layers, which is worthy of future research.

Acknowledgement:

This work was supported in part by National Natural Science Foundation of China No. 51605290, Shanghai Sailing Program No.16YF1405500.

Ruiliang Feng, <https://orcid.org/0000-0001-7867-3481>
 Lin Zhu, <https://orcid.org/0000-0002-1058-1289>
 Peng Li, <https://orcid.org/0000-0002-9974-1524>
 Xiangzhi Wei, <https://orcid.org/0000-0002-4541-0017>

REFERENCES

- [1] Buchbinder, D.; Meiners, W.; Pirch, N.; Wissenbach, K.; Schrage, J.: Investigation on reducing distortion by preheating during manufacture of aluminum components using selective laser melting, *Journal of Laser Applications*, 26(1), 2014, 012004. <http://doi.org/10.2351/1.4828755>
- [2] Carter, L.-N.; Martin, C.; Withers, P.-J.; Attallah, M.-M.: The influence of the laser scan strategy on grain structure and cracking behaviour in SLM powder-bed fabricated nickel superalloy, *Journal of Alloys and Compounds*, 615, 2014, 338-347. <http://doi.org/10.1016/j.jallcom.2014.06.172>
- [3] DebRoy, T.; Wei, H.-L.; Zuback, J.-S.; Mukherjee, T.; Elmer, J.-W.; Milewski, J.-O.; Beese, A.-M.; Wilson-Heid, A.; De, A.; Zhang, W.: Additive manufacturing of metallic components – Process, structure and properties, *Progress in Materials Science*, 92, 2018, 112-224. <http://doi.org/10.1016/j.pmatsci.2017.10.001>
- [4] Fieger, T.-V.; Sattler, M.-F.; Witt, G.: Developing laser beam welding parameters for the assembly of steel SLM parts for the automotive industry, *Rapid Prototyping Journal*, 24(8), 2018, 1288-1295. <https://doi.org/10.1108/RPJ-12-2016-0204>
- [5] Harun, W.-S.-W.; Kamariah, M.-S.-I.-N.; Muhamad, N.; Ghani, S.-A.-C.; Ahmad, F.; Mohamed, Z.: A review of powder additive manufacturing processes for metallic biomaterials, *Powder Technology*, 327, 2018, 128-151. <https://doi.org/10.1016/j.powtec.2017.12.058>
- [6] Järvinen, J.; Matilainen, V.; Li, X.; Piili, H.; Salminen, A.; Mäkelä, I.; Nyrhilä, O.: Characterization of effect of support structures in laser additive manufacturing of stainless steel, *Physics Procedia*, 56, 2014, 72-81. <https://doi.org/10.1016/j.phpro.2014.08.099>
- [7] Kempen, K.; Vrancken, B.; Bults, S.; Thijs, L.; Van Humbeeck, J.; Kruth, J. P.: Selective laser melting of crack-free high density M2 high speed steel parts by baseplate preheating, *Journal of Manufacturing Science and Engineering*, 136(6), 2014, 061026. <https://doi.org/10.1115/1.4028513>
- [8] Kruth, J.-P.; Froyen, L.; Van Vaerenbergh, J.; Mercelis, P.; Rombouts, M.; Lauwers, B.: Selective laser melting of iron-based powder, *Journal of Materials Processing Technology*, 149(1-3), 2004, 616-622. <https://doi.org/10.1016/j.jmatprotec.2003.11.051>
- [9] Lewis, G.-K.; Schlienger, E.: Practical considerations and capabilities for laser assisted direct metal deposition, *Materials & Design*, 21(4), 2000, 417-423. [https://doi.org/10.1016/S02613069\(99\)00078-3](https://doi.org/10.1016/S02613069(99)00078-3)

- [10] Lu, Y.; Wu, S.; Gan, Y.; Huang, T.; Yang, C.; Junjie, L.; Lin, J.: Study on the microstructure, mechanical property and residual stress of SLM Inconel-718 alloy manufactured by differing island scanning strategy, *Optics & Laser Technology*, 75, 2015, 197-206. <http://doi.org/10.1016/j.optlastec.2015.07.009>
- [11] Meiners, W.; Wissenbach, K.; Gasser, A.: Direct generation of metal parts and tools by selective laser powder remelting (SLPR). International Congress on Applications of Lasers & Electro-Optics, LIA, 1998, E31-E37.
- [12] Mercelis, P.; Kruth, J.: Residual stresses in selective laser sintering and selective laser melting, *Rapid Prototyping Journal*, 12(5), 2006, 254-265. <https://doi.org/10.1108/13552540610707013>
- [13] Meshprint, <https://www.youtube.com/watch?v=ARsYI4O0nkg>, Feng Ruiliang; Wei Xiangzhi.
- [14] Morgan, D.; Agba, E.; Hill, C.: Support structure development and initial results for metal powder bed fusion additive manufacturing, *Procedia Manufacturing*, 10, 2017, 819-830. <https://doi.org/10.1016/j.promfg.2017.07.083>
- [15] Mukherjee, T.; Zhang, W.; DebRoy, T.: An improved prediction of residual stresses and distortion in additive manufacturing, *Computational Materials Science*, 126, 2017, 360-372. <http://doi.org/10.1016/j.commatsci.2016.10.003>
- [16] Segonds, F.: Design By Additive Manufacturing: an application in aeronautics and defence, *Virtual and Physical Prototyping*, 13(4), 2018, 237-245. <https://doi.org/10.1080/17452759.2018.1498660>
- [17] Shiomi, M.; Osakada, K.; Nakamura, K.; Yamashita, T.; Abe, F.: Residual stress within metallic model made by selective laser melting process, *CIRP Annals*, 53(1), 2004, 195-198. [https://doi.org/10.1016/S0007-8506\(07\)60677-5](https://doi.org/10.1016/S0007-8506(07)60677-5)
- [18] Thijs, L.; Kempen, K.; Kruth, J.; Van Humbeeck, J.: Fine-structured aluminium products with controllable texture by selective laser melting of pre-alloyed AlSi10Mg powder, *Acta Materialia*, 61(5), 2013, 1809-1819. <https://doi.org/10.1016/j.actamat.2012.11.052>
- [19] Withers, P.-J.; Bhadeshia, H.-K.-D.-H.: Residual stress. Part 1 – Measurement techniques, *Materials Science and Technology*, 17(4), 2001, 355-365. <https://doi.org/10.1179/026708301101509980>
- [20] Withers, P.-J.; Bhadeshia, H.-K.-D.-H.: Residual stress. Part 2 – Nature and origins, *Materials Science and Technology*, 17(4), 2001, 366-375. <https://doi.org/10.1179/026708301101510087>
- [21] Yasa, E.; Deckers, J.; Kruth, J.; Rombouts, M.; Luyten, J.: Investigation of sectoral scanning in selective laser melting, *ASME 2010 10th Biennial Conference on Engineering Systems Design and Analysis*, American Society of Mechanical Engineers, 2010, 695-703.
- [22] Zhang, K.; Fu, G.; Zhang, P.; Ma, Z.; Mao, Z.; Zhang, D.: Study on the geometric design of supports for overhanging structures fabricated by selective laser melting, 12(1), 2019, 27. <https://dx.doi.org/10.3390%2Fma12010027>
- [23] Zhang, W.; Shi, Y.-S; Liu, B.; Xu, L.; Jiang, W.; Consecutive sub-sector scan mode with adjustable scan lengths for selective laser melting technology, *International Journal of Advanced Manufacturing Technology*, 41(7-8), 2009, 706-713. <https://doi.org/10.1007/s00170-008-1527-0>